Journal of the European Ceramic Society 44 (2024) 116813

Contents lists available at ScienceDirect

Journal of the European Ceramic Society

journal homepage: www.elsevier.com/locate/jeurceramsoc

Cold sintering of complex-shaped ceramic materials

Sonia Marín-Cortés [a,*], Mattia Biesuz [b,c,**], Subhadip Bhandari [d], Giorgia Franchin [d], Esther Enríquez [e], José F. Fernández [a], Vincenzo M. Sglavo [b,c]

[a] Instituto de Cerámica y Vidrio, ICV-CSIC, Kelsen, 5. Campus de Cantoblanco, Madrid 28049, Spain
[b] Department of Industrial Engineering, University of Trento, Via Sommarive 9, Trento 38123, Italy
[c] INSTM, Via G. Giusti 9, Firenze 50121, Italy
[d] Department of Industrial Engineering, University of Padova, Via Marzolo 9, Padova 35131, Italy
[e] Instituto de Óptica "Daza de Valdés" IO-CSIC, Serrano, 121, Chamartín, Madrid 28006, Spain

ARTICLE INFO

Keywords:
Complex shape
Cold sintering process
Hydroxyapatite
Diatomaceous earth
Construction/demolition waste materials
Zinc oxide

ABSTRACT

The present work explores for the first time the production of ceramic bodies with complex shape through the cold sintering process. Inspired by previous works on spark plasma sintering, a spacer accessory was designed to act as a removable mold. This proof-of-concept was tested with four different ceramic systems: biogenic hydroxyapatite, zinc oxide, *diatomaceous* earth and construction/demolition waste materials. In all cases, the density is comparable to that obtained by cold sintering of simpler disks. Moreover, the microstructure of the complex-shaped materials is substantially homogeneous in the entire component. Some distortions can be detected when comparing the spacer and sample shape, their control and modeling being a key challenge for future works.

1. Introduction

The cold sintering process (CSP) has attracted great interest over the last decade as it allows the densification of various ceramics at near room temperature (< 350 ºC), thus reducing the energy required for the process [1–6]. CSP involves the use of high pressures (hundreds of MPa) together with a transient liquid phase in "warm" conditions enabling mass transport and densification at temperatures even thousand degrees below the conventional sintering ones. The mechanisms are still partially a matter of discussion [7] and different phenomena can be activated, including water-induced plasticity [8]. In any case, CSP certainly involves the rearrangement, dissolution and re-precipitation of the ceramic particles. In general, CSP consists of three steps: i) mixing of the solid material with the solvent, ii) introduction of the mixture into the die, and iii) application of pressure for a certain time while maintaining the temperature at a specific level.

Due to the application of uniaxial pressure, CSP has some technological limitations. The most important ones are the low productivity of the process, which cannot be carried out continuously, and, at least so far, the possibility to obtain only small coin-shaped samples. No reports on more complex geometries by CSP have been found in the scientific literature, yet. The former limitation was recently addressed by Jabr et al. who showed that multiple samples can be processed in a single batch with good reproducibility [9]. The production of intricate shapes by CSP represents a scientific and technological challenge since the pressure applied uniaxially must be distributed uniformly throughout the sample to achieve a homogeneous material.

Regarding complex shapes by non-conventional sintering techniques, Manière al. [10] have pioneered a new approach applicable to spark-plasma sintering (SPS) [11–13] and flash-SPS [14]. The first study in 2016 used a sacrificial material that allowed the separation of the sample into two complex parts after sintering; however, the major drawbacks were the material loss from the sacrificial part and the limitation in thickness, being very difficult to produce thick bodies [11]. A year later, they overcame the shape limitation using an approach that consists of an intermediate layer between the sacrificial material and the base one, demonstrating the homogeneity of the resulting product [15]. Finally, in 2020, Hocquet et al. proposed to use an inert, temperature- and current-transmitting granulated bed where the previously formed complex-shape was introduced [16].

Inspired by such results obtained in SPS and flash-SPS, we questioned whether a similar approach could be applied also to the CSP, thus

* Corresponding author.
** Corresponding author at: Department of Industrial Engineering, University of Trento, Via Sommarive 9, Trento 38123, Italy.
E-mail addresses: sonia.marin@icv.csic.es (S. Marín-Cortés), mattia.biesuz@unitn.it (M. Biesuz).

https://doi.org/10.1016/j.jeurceramsoc.2024.116813
Received 26 March 2024; Received in revised form 25 June 2024; Accepted 5 August 2024
Available online 8 August 2024

enabling the manufacturing of complex ceramics structures. As proof of concept for validating its production, we investigated the use of CSP for Ca-deficient hydroxyapatite derived from biogenic sources (HA) [17], zinc oxide (ZnO), *diatomaceous* earth (DE) and recycled construction and demolition waste (CDW) [18]. This study presents both the design and fabrication of the mold, as well as the assessment of the resulting materials after the cold sintering process. The evaluation includes the density, geometry, profile evolution, and microstructure of the sintered materials.

2. Experimental procedures

The procedure proposed in the present work consists of the use of a mold, henceforth called "spacer" that can be produced by the additive manufacturing (AM) of an UV photocurable resin (Fig. 1a). The die used for CSP was loaded with the ceramic mixture; the spacer was then introduced, and finally additional ceramic mix was added before starting the experiment. In this way, the spacer was placed between two beds of ceramic powder (Fig. 1b). Finally, once the CSP was completed, the samples were removed from the die, with a positive and negative shape with respect to the used spacer (Fig. 1c). Different views of the designed spacers are reported in Figs. 1d and 1e. They consist of three concentrical cylinders (Fig. 1d), labeled hereinafter as *S1,* and a single ring with an external wall (Fig. 1e), called *S2*. The dimensions of these components were 13 mm in diameter, 3 mm in height, and 1 mm in thickness. Other shapes with edges that are neither perpendicular nor parallel to the applied uniaxial pressure were also tested (cone-shape shown in Fig. 1a) but the shape was not maintained during the process in such case. Therefore, only the results obtained with forms *S1* and *S2* are reported in the present work.

The material chosen to produce the spacer is of critical importance for the process, since it must possess the following characteristics: i) resistance to high pressures and mild temperature, ii) capacity to withstand acidic and alkaline conditions and iii) appropriate deformability that allows the spacer to adapt to the pressure and shrinkage of the sample while maintaining the shape integrity. Feasibility and cost-effective fabrication of the spacers are also important for their applicability: therefore, a simple and cheap process must be considered. For this reason, AM of a UV-photocurable resin was selected as it could meet all the above-mentioned requirements.

The CAD models for printing the spacer were designed using SolidWorks 2023 and then sliced with a layer thickness of 50 μm using PrusaSlicer 2.6.1; the initial layer exposure time was set to 20 s and then to 1 s for the subsequent layers. Subsequently, the samples were fabricated with the help of a masked stereolithography printer (Prusa SL1S, Prusa Research, Czech Republic), using a commercial resin from RobotFactory (RF resin-HT-Green, RobotFactory, Italy). The printed structures were then carefully removed from the printer, rinsed with alcohol to remove the uncured resin, and finally post-cured in the printer's curing and washing machine (Prusa CW1S, Prusa Research, Czech Republic) for about 2 min. The mechanical properties of the spacer were measured by using dog-bone samples (1 mm/min loading rate). To mimic the CSP process, the properties on the as-printed spacer and after 30 min annealing at 100 °C and 200 °C were measured. Tensile strength and elastic modulus were measured using an Instron 5969 machine (1 kN cell), following the ISO 527: Plastics — Determination of tensile properties.

The chosen materials for the viability study of the process were Ca-deficient hydroxyapatite derived from biogenic sources (HA) with crystallite size of 21 ± 4 nm [17], diatomaceous earth (DE) whose size ranges from a few microns to several tens of microns [19] (commercially available diatomite powder was provided by a Vietnamese mineral joint-stock company in Phu Yen), nanosized zinc oxide (NanoTek|r, CAS 1314–13–2, Thermo Scientific Chemicals) with average particle size

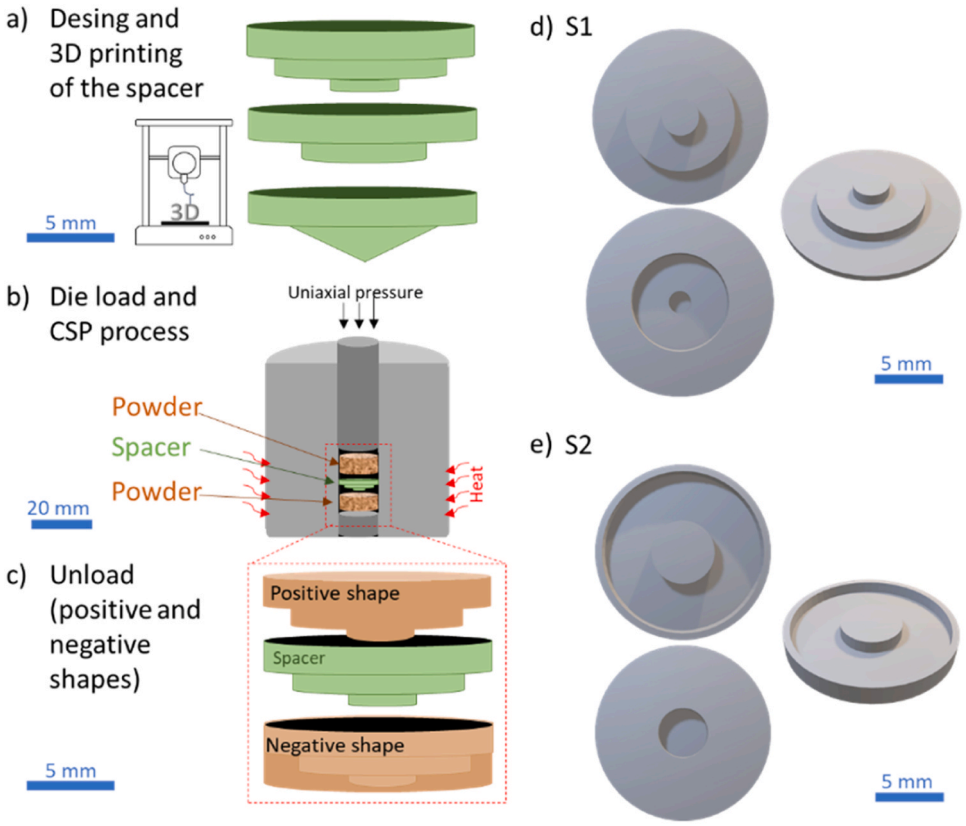

Fig. 1. Process workflow for obtaining complex-shaped ceramics by cold sintering: a) design and 3D printing of the spacer; b) die loading and cold-sintering process; c) realization of negative and positive shapes by die unloading. Different views of the S1 and S2 spacers are shown in d) and e).

equal to 45–89 nm and recycled construction and demolition waste (CDW) with micrometric particles around 8 ± 1 μm and submicrometric particles of 466 ± 45 nm as determined by DLS analysis. Details regarding processing and characterization of such materials as well as their use in conventional CSP can be found in previous works [18-20]. 0.1 M and 1 M acetic acid solution (ACS reagent, ≥ 99.7 %, CAS 64-19-7) was chosen as transient liquid phase for HA and ZnO respectively, while 3.5 M and 7 M KOH (J.T. Baker® ≥ 88 % CAS 1310-58-3) was used for *diatomaceous* earth and CDW. For the cold sintering process, a typical procedure was followed starting with the moistening of 0.5 g of powder with 40 wt% of solvent in an agate mortar. The paste-like mixture was then placed into a steel die (13 mm diameter) in the following order: bottom pressing punch, 0.5 g moistened powder, spacer, 0.5 g moistened powder and top pressing punch. In the case of ZnO, a graphite-containing acrylic resin coating (GRAPHIT 33, Kontakt Chemie) was sprayed on the surfaces of the top and bottom pressing punch and samples. This additional step was required because the material adhered strongly to the mold during CSP, losing its shape upon ejection. Therefore, ZnO powder was homogenized with the solvent and slightly manually pre-pressed for 3 s at 100 MPa. Once the powder acquired the shape (of the mold), it was unloaded and covered with two layers of graphite-containing coating. The covered pre-shaped moisturized powder was then pressed again in the die to follow the further CSP steps. The CSP was carried out by applying uniaxial pressure at 4 kN/min by a mechanical testing machine (MTS 810); the die was heated (20 °C/min) once the working pressure was reached by an external heating ring placed around the die. After CSP, the samples were naturally cooled to room temperature. The different solvents, applied pressures, temperatures and times are specified per each material in Table 1.

The density of the sintered samples was measured by the Archimedes' method using an analytical balance with 0.1 mg sensitivity and deionized water as buoyancy medium. At least three repetitions were performed for the density measurement. Theoretical density was addressed by He picnometry (AccyPyc 1330 TC, Micrometrics). These densities were used for the relative densities' calculation, being these 2.7 g/cm^3 for CDW, 3.1 g/cm^3 for HA, 5.6 g/cm^3 for ZnO and 2.3 g/cm^3 for DE. The shape of the CSP artefacts was analyzed using an Olympus LS digital microscope operating in bright field mode. The homogeneity and the microstructure of the materials were assessed by field emission scanning electron microscopy (FESEM) with a S-4700 Hitachi instrument operating at 20 kV. FESEM analyses were carried out on fresh fracture surface of selected samples.

3. Results and discussion

Fig. 2a shows the CSP samples. The different shapes are labeled as disk for the conventional shape and *S1* and *S2* for the two used spacers; a letter indicates the positive (P) and negative (N) shape (for example, *S1*P refers to the positive shape obtained by the spacer number 1). A 3D image of the CDW *S1*N sample is shown in Fig. 2b. One can observe that the process allowed to obtain CSP components with geometries different from the usual disks. It is important to point out that one of the sides of the obtained shapes (negative or positive, depending on the need) acts as sacrificial part to obtain the same sintering strain, thus allowing to have the same displacement in the whole sample directions. Moreover, to decrease the production costs, a cheaper powder with similar sintering behavior could be used as sacrificial element. The relative density of each sample is shown in Table 2. The results suggest that the spacer did not impact negatively on densification and no substantial differences can be identified when comparing the complex shapes and the disk samples. The process appears quite reproducible and can be extended to different compositions as demonstrated by the fact that positive results were obtained by using four dissimilar ceramic systems.

Table 1
Conditions (solvent, applied pressure, temperature and dwell time) used for the different materials (CDW, HA and DE) during CSP.

	Solvent	Applied pressure (MPa)	Temperature (°C)	Dwell time (min)
CDW	7 M KOH	500, 600	100, 200	30
HA	0.1 M acetic acid	600	200	15
DE	3.5 M KOH	300	150	12
ZnO	1 M acetic acid	500	140	15

As for the mechanical properties recorded for the resin (see Supplementary information), the starting elastic modulus is ~ 240 MPa, which increases to ~ 280 MPa at 100 °C and reaches 1320 MPa at 200 °C. Similarly, the resistance increases with the annealing temperature and is equal to 7.2 ± 0.9, 8.2 ± 1.7 and 12.3 ± 4.9 MPa for as-printed samples and for the samples annealed at 100 and 200 °C, respectively. The sample evolution during the thermal treatment is fully consistent with the thermosetting nature of the resin, which completes the cross-linking process while heated. This behavior is of special interest in the present application since it allows the shape of the spacer to remain stable under the high pressure applied during the process.The shape of some samples was recorded with an optical microscope and compared with the employed spacer. Fig. 3a–c correspond to *S1* samples and *S2* positive and negative specimens, respectively. One can observe that the final geometry of the CSP material is quite different compared with that of the spacers and, as such, future works are needed to identify and model such distortions. In particular, all features in the vertical direction appear compressed between 10 % and 60 % as a result of the directional shrinkage upon CSP. This variation among the samples relies on the specific behavior of the used material which is an important parameter to be considered when modeling the deviation of the shapes. Another type of geometrical defect can be identified in Fig. 2a for the CDW material (also shown in the 3D image of the same sample as in Fig. 2b). In detail, one can observe a buckling of the spacer induced by its compression, which led to a weave-like texture. These results reinforce the importance of the resin selection for the spacer, since it should be able to adapt to the process without losing the shape as observed here; at the same time, it must be flexible enough to adapt to the sample shrinkage without damaging the sample. This fact should be explored in further works, together with the effect of the spacer thickness, the filling procedure of the die, the amount of ceramic powder to minimize and control geometrical distortion and to eventually design the spacer for the final desired shape accounting for such deformation.

When complex shapes obtained by uniaxial pressing are considered, the critical point is the material homogeneity, which reflects the distribution of the applied pressure. Final homogeneity of the microstructure is a good proof of an even distribution of the applied pressure and, therefore, homogeneous densification. The fresh fracture surface micrographs of the S1N shape for each material are reported in Fig. 4. Two areas were chosen, namely, A - edge and B - center of the sample (Fig. 4). In the case of CDW, microparticles corresponding to material relicts appear embedded within the Ca-rich nanostructured matrix formed after the cold sintering. HA shows a well-densified microstructure similar to those reported in the literature for the same material [20]. Finally, in the case of DE material, flattened and oriented grains are observed. This effect corresponds to the powder deformation induced by CSP and has been already discussed in a previous work [19].

The key result here is that no substantial differences can be identified in the sample density/microstructure in the different regions (center and edge) of the component although its thickness changes substantially. One should note that such result could not be possible without the use of a spacer and sacrificial powder, for instance just by shaping the punch with a complex-shape. In fact, regions of the sample with different thicknesses would require different sintering displacements to achieve the same strain and microstructure. This cannot be obtained using a rigid punch where the displacement is the same along the cross-section.

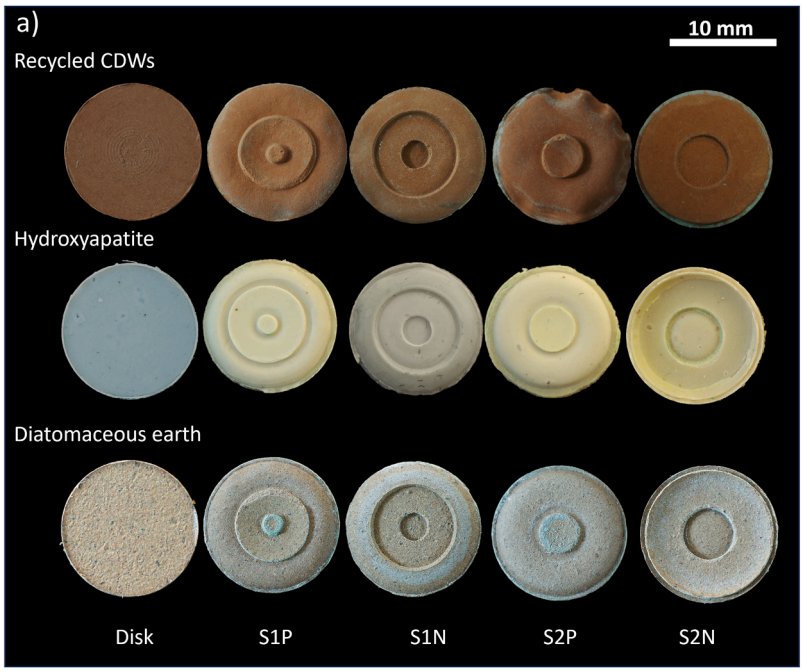

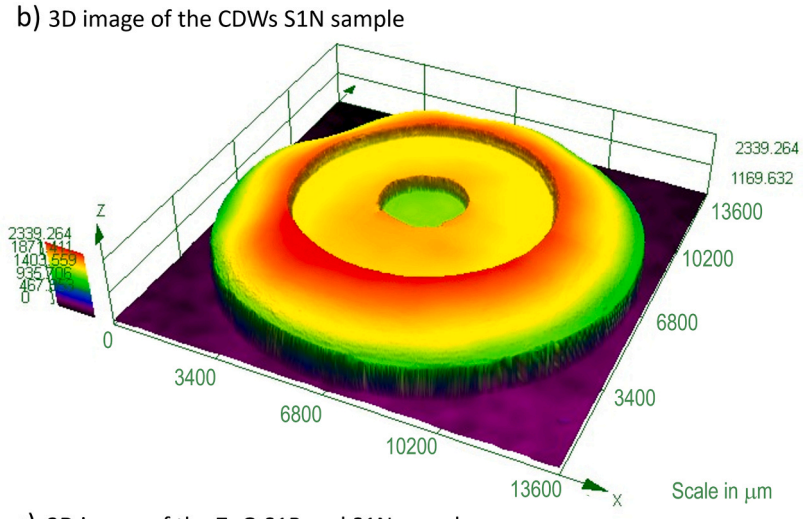

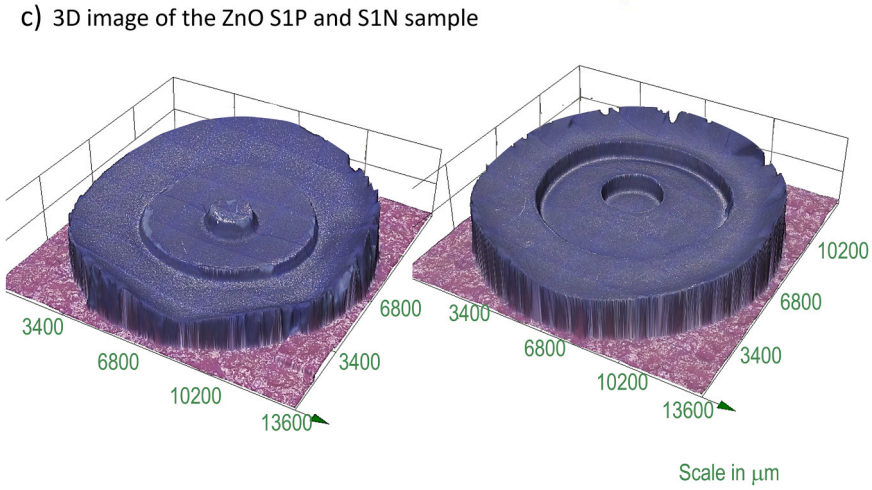

Fig. 2. a) Photographs of disks and complex-shaped samples obtained by CSP. In the case of CDW, the disk and S2N were obtained at 200 °C under 600 MPa, the remaining having been produced at 100 °C under 500 MPa. b) 3D image of CDW S1N sample. c) 3D image of ZNO S1P and S1N covered with graphite-containing acrylic resin spray coating. The reported numbers are in microns. The reported numbers are in microns.

Table 2
Relative bulk density of the different complex-shaped ceramics obtained by CSP. In the case of CDW, the disk and S2N shapes were produced at 200 °C under 600 MPa, the others at 100 °C under 500 MPa.

	ρ_{disk} (%)	ρ_{S1P} (%)	ρ_{S1N} (%)	ρ_{S2P} (%)	ρ_{S2N} (%)
CDW	88.8 ± 0.5	85.6 ± 0.5	84.6 ± 0.5	85.7 ± 0.5	87.5 ± 0.5
HA	74.7 ± 1.2	76.9 ± 1.2	74.2 ± 1.2	72.3 ± 1.1	77.0 ± 1.2
DA	92.2 ± 0.5	90.1 ± 0.5	89.9 ± 0.5	84.2 ± 0.5	89.6 ± 0.5
ZnO	-	94.4 ± 0.2	94.0 ± 0.2	-	-

4. Conclusions

Dense ceramics with complex shapes were obtained by the cold sintering process for the first time. This proof of concept was demonstrated using different ceramics such as hydroxyapatite, construction and demolition wastes, ZnO, and *diatomaceous* earth. The advantages of this solution are based on the versatility of the spacer design which is produced by additive manufacturing of a photocurable resin. It is important to point out that the low-temperature treatment used in CSP allows the use of organic compounds as spacers. Very interestingly, the samples with complex-shapes present homogeneous microstructure and density similar to those of coin-like specimens. Future studies are needed to optimize the process and to reduce/control the distortions induced by uniaxial pressing.

Summary of novel conclusions

- For the first time, complex-shaped ceramics were obtained by the cold sintering process.

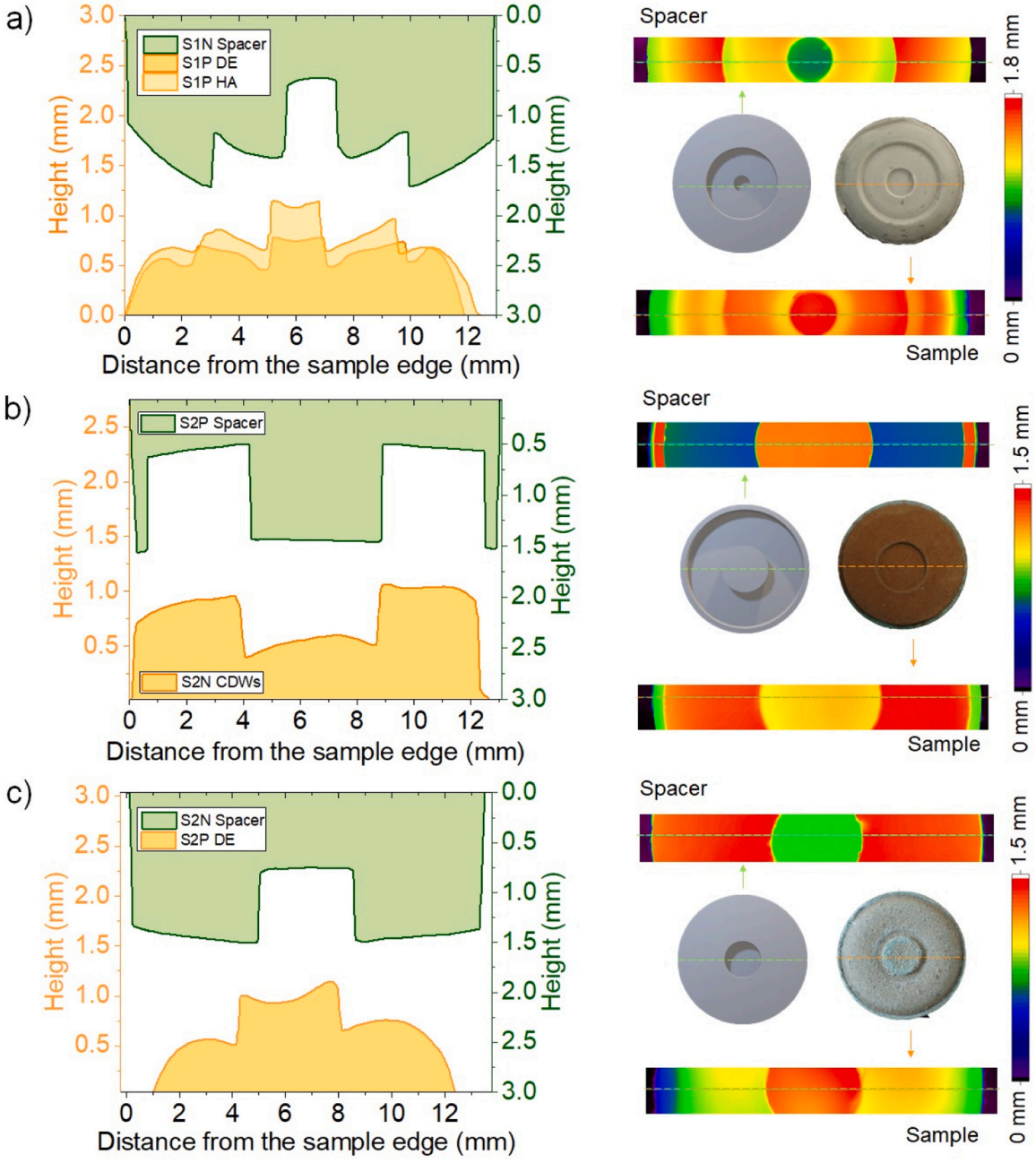

Fig. 3. Profiles for *S1* (a), *S2* positive (b), S2 negative (c) spacers and corresponding samples.

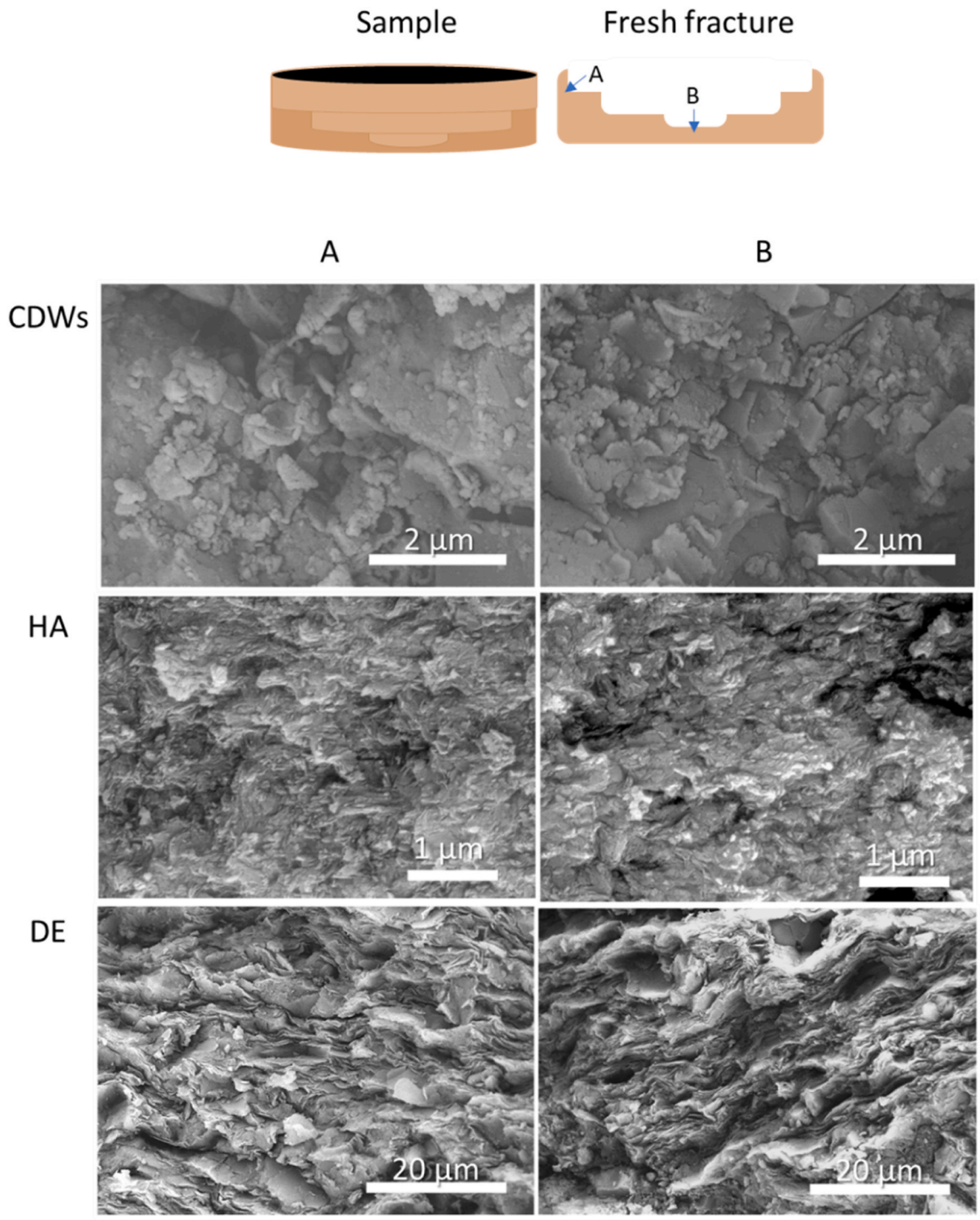

Fig. 4. Microstructure detected in different parts (A: left, B: center) of fresh fracture samples.

- To achieve this, polymeric spacers with the desired shape were designed and obtained by additive manufacturing. These spacers were introduced in the powder during the cold sintering procedure.
- Four different ceramics were tested to validate the procedure: biogenic hydroxyapatite, *diatomaceous* earth, construction/demolition waste materials, and ZnO.
- The obtained complex-shaped samples show densities comparable to the disk-shaped ones. The microstructure through the sample was substantially homogeneous.
- This procedure constitutes a cost-effective solution for the realization of complex-shaped ceramics by cold sintering.

CRediT authorship contribution statement

Mattia Biesuz: Writing – original draft, Validation, Supervision, Investigation, Formal analysis, Data curation, Conceptualization. **Subhadip Bhandari:** Writing – original draft, Validation, Methodology, Investigation, Conceptualization. **Sonia Marín Cortés:** Writing – review & editing, Writing – original draft, Validation, Methodology, Investigation, Formal analysis, Data curation, Conceptualization. **José F. Fernández:** Writing – review & editing, Resources, Project administration, Funding acquisition. **Vincenzo M. Sglavo:** Writing – review & editing, Validation, Supervision, Resources, Project administration,

Funding acquisition. **Giorgia Franchin:** Writing – review & editing, Validation, Supervision, Project administration, Investigation, Formal analysis, Conceptualization. **Esther Enríquez:** Supervision.

Declaration of Competing Interest

The authors declare that they have no known competing financial interests or personal relationships that could have appeared to influence the work reported in this paper.

Acknowledgments

The authors gratefully acknowledge the financial support of the European Union's Horizon 2020 Research and Innovation Programs ICEBERG (No. 869336) for their financial support. Subhadip Bhandari gratefully acknowledges the CARIPARO Foundation, Padova, Italy, for his Ph.D. scholarship. This work was supported by the Spanish Ministry for Science and Innovation (MCIN) under the project PID2020-114192RB-C41. UNITN is also acknowledged for the financial support and the used facilities.

Appendix A. Supporting information

Supplementary data associated with this article can be found in the online version at doi:10.1016/j.jeurceramsoc.2024.116813.

References

[1] J. Guo, H. Guo, A.L. Baker, M.T. Lanagan, E.R. Kupp, G.L. Messing, C.A. Randall, Cold sintering: a paradigm shift for processing and integration of ceramics, Angew. Chem. - Int. Ed. 55 (2016) 11457–11461, https://doi.org/10.1002/anie.201605443.

[2] J. Guo, R. Floyd, S. Lowum, J.-P. Maria, T. Herisson de Beauvoir, J.-H. Seo, C. A. Randall, Cold sintering: progress, challenges, and future opportunities, Annu. Rev. Mater. Res. 49 (2019) 275–295, https://doi.org/10.1146/annurev-matsci-070218-010041.

[3] A. Ndayishimiye, M.Y. Sengul, S.H. Bang, K. Tsuji, K. Takashima, T. Hérisson de Beauvoir, D. Denux, J.-M. Thibaud, A.C.T. van Duin, C. Elissalde, G. Goglio, C. A. Randall, Comparing hydrothermal sintering and cold sintering process: mechanisms, microstructure, kinetics and chemistry, J. Eur. Ceram. Soc. 40 (2020) 1312–1324, https://doi.org/10.1016/j.jeurceramsoc.2019.11.049.

[4] S. Grasso, M. Biesuz, L. Zoli, G. Taveri, A.I. Duff, D. Ke, A. Jiang, M.J. Reece, A review of cold sintering processes, Adv. Appl. Ceram. 119 (2020) 115–143, https://doi.org/10.1080/17436753.2019.1706825.

[5] A. Galotta, V.M. Sglavo, The cold sintering process: a review on processing features, densification mechanisms and perspectives, J. Eur. Ceram. Soc. 41 (2021) 1–17, https://doi.org/10.1016/j.jeurceramsoc.2021.09.024.

[6] C. Vakifahmetoglu, L. Karacasulu, Cold sintering of ceramics and glasses: a review, Curr. Opin. Solid State Mater. Sci. 24 (2020) 100807, https://doi.org/10.1016/j.cossms.2020.100807.

[7] M. Biesuz, G. Taveri, A.I. Duff, E. Olevsky, D. Zhu, C. Hu, S. Grasso, A theoretical analysis of cold sintering, Adv. Appl. Ceram. 119 (2020) 75–89, https://doi.org/10.1080/17436753.2019.1692173.

[8] J. Gonzalez-Julian, K. Neuhaus, M. Bernemann, J. Pereira da Silva, A. Laptev, M. Bram, O. Guillon, Unveiling the mechanisms of cold sintering of ZnO at 250 °C by varying applied stress and characterizing grain boundaries by Kelvin Probe Force Microscopy, Acta Mater. 144 (2018) 116–128, https://doi.org/10.1016/j.actamat.2017.10.055.

[9] A. Jabr, H.N. Jones, A.P. Argüelles, S. Trolier-McKinstry, C. Randall, R. Bermejo, Scaling up the cold sintering process of ceramics, J. Eur. Ceram. Soc. 43 (2023) 5319–5329, https://doi.org/10.1016/j.jeurceramsoc.2023.04.061.

[10] C. Manière, U. Kus, G. Chevallier, A. Weibel, L. Durand, J. Huez, D. Delagnes, C. Estournès, How to overcome the main challenges of SPS technology: reproducibility, multi-samples and elaboration of complex shapes, in: Spark Plasma Sintering, Elsevier, 2019, pp. 77–108, https://doi.org/10.1016/B978-0-12-817744-0.00003-9.

[11] C. Manière, L. Durand, A. Weibel, G. Chevallier, C. Estournès, A sacrificial material approach for spark plasma sintering of complex shapes, Scr. Mater. 124 (2016) 126–128, https://doi.org/10.1016/j.scriptamat.2016.07.006.

[12] C. Manière, E. Torresani, E.A. Olevsky, Simultaneous spark plasma sintering of multiple complex shapes, Materials 12 (2019) 1–14, https://doi.org/10.3390/ma12040557.

[13] C. Manière, L. Durand, A. Weibel, C. Estournès, Spark-plasma-sintering and finite element method: from the identification of the sintering parameters of a submicronic α-alumina powder to the development of complex shapes, Acta Mater. 102 (2016) 169–175, https://doi.org/10.1016/j.actamat.2015.09.003.

[14] C. Manière, G. Lee, E.A. Olevsky, Flash sintering of complex shapes, Appl. Mater. Today 26 (2022) 101293, https://doi.org/10.1016/J.APMT.2021.101293.

[15] C. Manière, E. Nigito, L. Durand, A. Weibel, Y. Beynet, C. Estournès, Spark plasma sintering and complex shapes: the deformed interfaces approach, Powder Technol. 320 (2017) 340–345, https://doi.org/10.1016/j.powtec.2017.07.048.

[16] S. Hocquet, V. Dupont, F. Cambier, F. Ludewig, N. Vandewalle, Densification of complex shape ceramics parts by SPS, J. Eur. Ceram. Soc. 40 (2020) 2586–2596, https://doi.org/10.1016/J.JEURCERAMSOC.2019.10.038.

[17] A. Galotta, F. Agostinacchio, A. Motta, S. Dirè, V.M. Sglavo, Mechanochemical synthesis and cold sintering of mussel shell-derived hydroxyapatite nano-powders for bone tissue regeneration, J. Eur. Ceram. Soc. 43 (2023) 639–647, https://doi.org/10.1016/j.jeurceramsoc.2022.09.024.

[18] S. Marín-Cortés, M. Fernández-Álvarez, A. Moure, J.F. Fernández, E. Enríquez, Chemometric-driven quantification of construction and demolition waste using Raman spectroscopy and SWIR: enhancing sustainability in the ceramic sector, Resour. Conserv. Recycl. 199 (2023) 107259, https://doi.org/10.1016/J.RESCONREC.2023.107259.

[19] A. Galotta, E. Giust, M. Bortolotti, G.D. Sorarù, V.M. Sglavo, M. Biesuz, Cold sintering of diatomaceous earth, J. Am. Ceram. Soc. 104 (2021) 4329–4340, https://doi.org/10.1111/JACE.17863.

[20] A. Galotta, F. Agostinacchio, A. Motta, S. Dirè, V.M. Sglavo, Mechanochemical synthesis and cold sintering of mussel shell-derived hydroxyapatite nano-powders for bone tissue regeneration, J. Eur. Ceram. Soc. 43 (2023) 639–647, https://doi.org/10.1016/j.jeurceramsoc.2022.09.024.